

1 **Prediction and validation of the three-dimensional structure of**  
2 **glucokinase-1 from *Phytophthora infestans***

3

4 **Liara Villalobos-Piña,<sup>1, 2\*</sup>, Ascanio Rojas<sup>2\*</sup>, Héctor Acosta<sup>3\*</sup>**

5

6 <sup>1</sup>Laboratorio de Fisiología. Departamento de Biología, Facultad de Ciencias, Universidad  
7 de Los Andes, Mérida 5101, Venezuela.

8 <sup>2</sup>Centro de Cálculo de la Universidad de Los Andes (CeCalCULA), Mérida 5101,  
9 Venezuela.

10 <sup>3</sup>Laboratorio de Enzimología de Parásitos, Departamento de Biología, Facultad de Ciencias,  
11 Universidad de Los Andes, Mérida 5101, Venezuela.

12

13 **\*Corresponding author Tel.:** +58 4165757494. e-mail addresses: [liaravipi@gmail.com](mailto:liaravipi@gmail.com)  
14 (Liara Villalobos-Piña)

15

16

17

18

19

20

21

22

23

24

25

26

27

28

29

30

31

32

33

34

35

## 36 Abstract

37 According to its primary structure, the [PITG\_06016] gene encodes for one of the 7  
38 glucokinases present in *Phytophthora infestans* (*PiGlcK-1*), the causal agent of late blight  
39 disease. Currently, there are no structural studies of any of its enzymes, being the  
40 determination of the three-dimensional (3D) structure of *PiGlcK-1* a necessary contribution  
41 in the deduction of its functions, its interaction with ligands, and possible regulatory  
42 mechanisms. In this work we present the first structural model obtained by *in silico* tools  
43 for *PiGlcK-1*. For the prediction of this model, different algorithms were used to find the  
44 best annealing, refinement, and qualitative evaluation of them. A structural comparison of  
45 the predicted model with other structures of crystallized kinase enzymes allowed us to  
46 identify the regions of interaction with their classical substrates (glucose and ATP), as well  
47 as to identify the amino acid residues involved in the binding of other substrates such as  
48 fructose and ADP. In addition, we propose a possible recognition region of PPI, an  
49 activator of kinase activity that includes the GXGE motif, conserved in enzymes of the  
50 ribokinase (RK) family, which distinguishes this *PiGlcK-1* from a classical glucokinase.  
51 Accordingly, these findings suggest PPI-binding motif as potential targets for the  
52 development of inhibitors of *PiGlcK-1* activity.

53

54 **Keywords:** *Phytophthora infestans*, glucokinase, modeling structural, molecular docking,  
55 PPI-binding motif.

56

57

58

59

## 60 **Introduction**

61 *Phytophthora infestans* is the causal agent of late blight disease, which affects potato and  
62 tomato crops worldwide, causing significant economic losses in the production of these  
63 crops [1]. The (PITG\_06016) gene codes for one of the 7 glucokinases present in this  
64 phytopathogen [2]. This glucokinase, known as *PiGlcK-1*, is very important due to its high  
65 degree of expression precisely at the infectious stages of its life cycle [3]. *PiGlcK-1* was  
66 also the first *P. infestans* glucokinase to be biochemically characterized, and based on its  
67 sequence, it would belong to the glucokinase A group of the hexokinase family. Certainly,  
68 the characterization of *PiGlcK-1* has revealed the versatility of this enzyme in the  
69 phosphorylation of both glucose and fructose, as well as in the utilization of ATP, ADP,  
70 and PPi as phosphoryl donors [4].

71 These findings raise the need for further structural analyses on *PiGlcK-1*. In this sense, a  
72 better understanding of the three-dimensional (3D) structure of this protein, as well as the  
73 spatial description of the possible binding sites to various ligands would contribute to the  
74 knowledge of potential targets for the design of inhibitors of the enzymatic activity of  
75 *PiGlcK-1*, a key enzyme in the metabolism of *P. infestans*.

76 However, experimental determination of protein structures remains a costly and time-  
77 consuming challenge. In fact, to date no *P. infestans* enzyme has been structurally  
78 characterized. In contrast, bioinformatics tools offer an alternative that allows prediction of  
79 3D protein structures by molecular dynamics and homology modeling which is faster,  
80 cheaper, and highly reliable. The reliability of these tools is based on the use of databases

81 of solved protein structures that can serve as homology templates in the simulation and  
82 structural prediction of proteins [5].

83 In this work we present the first model obtained by *in silico* tools of the 3D structure of  
84 *PiGlcK-1* and the binding sites to its classical substrates glucose and ATP, as well as to  
85 fructose and ADP, and a possible binding site to PPI that is propose as a promising target  
86 for the design of an inhibitor of this enzyme.

87

## 88 **Materials and methods**

### 89 **Sequence availability**

90 The amino acid sequence of the protein *PiGlcK-1* was obtained from the NCBI database  
91 under accession number XP\_002998228.

92

### 93 **Structural analysis of *PiGlcK-1* protein**

94 The 3D structure of the protein *PiGlcK-1* was obtained by homology modeling using the  
95 Phyre2 [6], LOMETS [7] and I-TASSER [8] algorithms. Each simulation obtained was  
96 refined with Galaxy Refine [9] to the maximum allowed, in some cases up to three times.  
97 Validation of structural stability was performed by qualitative evaluation by ModFOLD6  
98 [10] and by Ramachandran plot analysis obtained with SwissModel [11]. The topology of  
99 the *PiGlcK-1* model was obtained with Pro-origami [12]. Visualization and editing of the  
100 models was performed in Chimera 1.15.1 [13].

101

### 102 **Docking**

103 Molecular docking was carried out in SwissDock [14] using the refined *PiGlcK-1* model  
104 and substrates obtained from PubChem [15]: glucose (107526), fructose (2723872),  
105 ATP/Mg<sup>+2</sup> (5957), ADP/Mg<sup>+2</sup> (6022), and PPI/Mg<sup>+2</sup> (644102). In each case, the best  
106 energetic fits, such as model interaction energy of the complex bound to *PiGlcK-1* and  
107 *fullfitness* values, were evaluated. Model visualization and editing was performed with  
108 Chimera 1.15.1 [13].

109

## 110 **Results**

### 111 **Tertiary structure modeling**

112 The models obtained from the structure of *PiGlcK-1* in three different algorithms (Phyre2,  
113 LOMETS and I-TASSER) were highly satisfactory, obtaining overall scores greater than  
114 0.4 and a p-value cut-off of less than 0.001 which are considered very good (Table 1).

115 In each case, the models were refined until the best structure was obtained, according to  
116 the Ramachandran graph, with the model yielded by Phyre2 being the most suitable due to  
117 its higher stereochemical quality, with 97.95% of the amino acids in Ramachandran regions  
118 favored, making it the potentially reliable and good quality 3D model of the *PiGlcK-1*  
119 protein for this work (Figure 1).

120 The predicted model indicated that the monomeric structure was composed of two  
121 domains, a small one including residues 7 to 128, and a large domain formed by residues  
122 135 to 343. Both domains were consecutively labeled from N-terminal to C-terminal and  
123 linked by a hinge (Figure 2).

124 The topology obtained by Pro-Origami (S1Figure) showed that the small domain  
125 consists of 4  $\alpha$ -helices and 7  $\beta$ -sheet distributed in two mixed central sheets; one of them

126 of 5 stranded  $\beta$  ( $\beta$ 1,  $\beta$ 2,  $\beta$ 3,  $\beta$ 4 and  $\beta$ 7) with  $\beta$ 2 anti-parallel to the rest and another one  
127 formed by 2  $\beta$ -sheet ( $\beta$ 5 and  $\beta$ 6) anti-parallel to each other. These sheets are flanked by 4  
128  $\alpha$ -helix ( $\alpha$ 1,  $\alpha$ 2,  $\alpha$ 3 y  $\alpha$ 4).

129 On the other hand, the large domain consists of 10  $\alpha$ -helices and 6  $\beta$ -sheet organized in  
130 a single mixed central sheet containing all 6 chains  $\beta$  ( $\beta$ 8,  $\beta$ 9,  $\beta$ 10,  $\beta$ 11,  $\beta$ 12 and  $\beta$ 13) with  
131  $\beta$ 8 and  $\beta$ 10 anti-parallel to the rest. This sheet is flanked by 10  $\alpha$ -helices ( $\alpha$ 5,  $\alpha$ 6,  $\alpha$ 7,  $\alpha$ 8,  
132  $\alpha$ 9,  $\alpha$ 10,  $\alpha$ 11,  $\alpha$ 12,  $\alpha$ 13 and  $\alpha$ 14) (S1).

133

#### 134 **Molecular docking studies**

135 In order to know the active site of the *Pi*GlcK-1 a docking was performed with its classic  
136 substrates glucose and ATP-Mg<sup>2+</sup>. This analysis showed that the glucose binding site is in  
137 the large domain while the ATP binding site is in the small domain; both molecules interact  
138 with an extensive network of hydrogen bonds within the active site (Figure 3). These  
139 results were compared with those obtained by crystallography for GlcK from *Escherichia*  
140 *coli* (EcGlcK) (PDB: 1SZ2), GlcK from *Trypanosoma cruzi* (TcGlcK) (PDB: 2Q2R), and  
141 the 3D model of the complex GlcK-Mg<sup>2+</sup>-ATP-glucose (GMAG) of human [16].

142 In this sense, the hydrogen bonds with the best values of  $\Delta G$  y *fullfitness* were obtained  
143 from the residues Glu 209; Glu 176, His 179; Asn 117, and Asp 118 with atoms O1; O2; O3  
144 and O4 of glucose with a  $\Delta G$  of -5.27 and a *fullfitness* value of -1746.84 (Figure 3).  
145 Whereas for the  $\beta$ -phosphoryl group of ATP, the best values were obtained with the amino  
146 acids Thr 15 and Asn 16, and the  $\gamma$ -phosphoryl interacting with the O6 atom of glucose  
147 with an energy of -11.69 kcal/mol and a *fullfitness* value of -2187.34 (Figure 3). Notably,

148 all the interacting residues described above are highly conserved in group A GlcKs from  
149 diverse organisms [4].

150

### 151 **Fructose-binding site**

152 We have previously demonstrated experimentally that *PiGlcK-1* is able to phosphorylate  
153 other sugars such as fructose [4]. To identify a possible binding site for this hexose, we  
154 compared the fructose binding site with that of glucose, obtaining that this sugar interacts  
155 with the same amino acid residues described for glucose in this work. Fructose binding, as  
156 for glucose, occurred in the large domain and hinge region of *PiGlcK-1* with an energy of -  
157 5.742 kcal/mol and a *fullfitness* value of -1728.80 (Figure 4A).

158

### 159 **Identification of ADP and PPi-binding site**

160 One of the particularities of *PiGlcK-1* is to use ADP or PPi as a phosphoryl donor for the  
161 formation of hexose-6-phosphate. Additionally, PPi proved to be an efficient activator of  
162 *PiGlcK-1* when the phosphoryl donors are ATP or ADP [4]. Initially, we determined the  
163 binding site of ADP, by performing a docking of this ligand to *PiGlcK-1*, finding that it  
164 indeed interacts with the same residues present in the small domain described for ATP with  
165 an energy of -10.59 kcal/mol and a *fullfitness* of -2041.78 (Figure 4B).

166 For its part, the best docking obtained for *PiGlcK-1*-PPi was located in a region other  
167 than the ATP-binding and ADP-binding region, this being the larger domain with an energy  
168 of -5.425 kcal/mol and a *fullfitness* of -2150.14 (Figure 5A). Interestingly, the amino acids  
169 involved in this interaction, Lys 282, Thr 180 and Arg 210 (Figure 5B), have already been  
170 reported for the PPi-dependent kinase from *Thermotoga maritima* [17]. Markedly, *PiGlcK-*  
171 1 also possesses the conserved GXGD(E) motif consisting of Gly 156, Leu 157, Gly 158

172 and Glu 159. This motif has been described in the ADP-dependent kinases of the  
173 Ribokinase family (RK) [18,19] in a region very close to the previously described PPI-  
174 binding motif, thus suggesting that residues involved in phosphoryl binding in RKs could  
175 also be participating in interaction with PPI in *PiGlcK-1*. However, although this motif is  
176 described to bind ADP, in our case this is not possible since the ADP would be in a region  
177 other than the hinge region.

178

## 179 **Discussion**

180 Using molecular modeling and simulation methods, we constructed the 3D  
181 structural model for *PiGlcK-1*. This model was validated and structurally compared with  
182 kinase enzymes of the HK and GlcK A family from other organisms, verifying that  
183 *PiGlcK-1* folds similarly to HK from yeast [20], HK from human [16] and GlcK from *E.*  
184 *coli* [21], whose crystallographic structures have already been described.

185 With our model of *PiGlcK-1* we were able to verify that the monomeric structure of the  
186 enzyme is highly conserved as it is composed of a large domain and a small domain  
187 connected to each other by a hinge region; both domains are made of  $\beta$ -sheet, flanked by  $\alpha$ -  
188 helices, and between both lobes a cavity where the catalytic site is located, similar to many  
189 hexose kinases from several phylogenetically unrelated organisms [16, 20, 21].

190 Molecular docking assays on *PiGlcK-1* verified that ATP and glucose do indeed  
191 interact via hydrogen bonds with the residues that form the active site of the protein, as it  
192 has been described for several hexokinases and glucokinases [20]. The glucose binding site  
193 comprises well-conserved residues in the hinge region (Asp 118, Asn 117) and the large  
194 domain (Glu 176, His 179, Glu 209). In contrast, ATP binds mainly to residues Asp 11, Thr



195 15, and Asn 16 of the small domain with the  $\gamma$ -phosphoryl group pointing toward the hinge  
196 region, as it has been reported for hexokinase and glucokinase enzymes from various  
197 organisms [20].

198 In each case, the calculated distances between the enzyme and its substrates were made  
199 on a rigid model, so the value of these exceeds 2 Å. However, it is worth considering the  
200 intrinsic flexibility of different GlcKs [20, 21] which has reached in *Pyrococcus furiosus* a  
201 displacement of 12 Å when comparing the protein in the presence and absence of glucose  
202 [22]. Thus, the interactions between the ligands and the amino acid residues in *PiGlcK-1*  
203 proposed here are highly consistent with the crystallographic structures mentioned above.

204 Furthermore, it has been observed that fructose from the plant, like glucose, is important  
205 for the metabolism of *P. infestans* during the establishment of infection, where its  
206 concentration in potato and tomato leaves is higher than that of glucose [23-25]. Due to the  
207 absence of a specialized fructokinase (EC 2.7.1.4) in *P. infestans* [25] this sugar must be  
208 obligatorily phosphorylated by *PiGlcK-1*.

209 Therefore, having corroborated in the docking of *PiGlcK-1* with glucose and ATP that  
210 these were located in the active site, interacting with amino acid residues conserved for  
211 other kinases, docking was carried out for fructose as well as for the phosphoryl donors  
212 ADP and PPi.

213 As expected, both fructose and ADP are able to form hydrogen bonds with the same  
214 amino acid residues described for their glucose and ATP pairs, respectively, validating that  
215 these can be utilized under certain physiological conditions during the life cycle of *P.*  
216 *infestans*. In this case, when glucose or ATP concentrations are low, *P. infestans* could  
217 obtain energy and/or NADPH through glycolysis or the pentose phosphate pathway, which

218 would function from the use of fructose and ADP, thus ensuring that the enzyme remains  
219 active during the establishment of infection, regardless of the fact that the availability of  
220 glucose or ATP is compromised.

221 On the contrary, the docking for P<sub>Pi</sub>, located in the large domain, close to the hinge  
222 region but in a site different from the ATP/ADP binding site (Figure 5A), would explain its  
223 role as an activator of PiGlcK-1 activity in the presence of ATP or ADP [4]. This activating  
224 role of P<sub>Pi</sub> could be related to a possible stabilization of a catalytically more active  
225 conformation of the enzyme, although more assays are needed to corroborate this  
226 hypothesis.

227 The importance of the role played by P<sub>Pi</sub> in *P. infestans* has been evidenced by several  
228 facts such as : i) *P. infestans* can produce P<sub>Pi</sub> through multiple biosynthesis and hydrolysis  
229 reactions carried out in this phytopathogen [26], ii) it expresses significant levels of several  
230 enzymes relevant to its energy metabolism which are P<sub>Pi</sub>-dependent, such as pyruvate  
231 phosphate dikinase (PPDK), 6-phosphofructose-1-kinase (PFK), and 6-phosphofructose-2-  
232 kinase(PFK2) [3,25,27], iii) it has been suggested that the majority of the glycolytic flux in  
233 the hyphal sporulation stage of *Phytophthora cinnamomi* occurs via PPDK [28], iv) PPDK  
234 may play a more relevant role than PYK in glycolysis of *P. infestans* due to a higher  
235 expression of PPDK relative to PYK [29], v) pyrophosphate stimulates calcium uptake in  
236 diverse organisms including *P. infestans*, which is required for its growth and development  
237 [30]

238 Although the true value of P<sub>Pi</sub> in the metabolism of *P. infestans* remains to be clarified,  
239 it is important to consider the binding motif of this ligand when designing potential  
240 inhibitors of PiGlcK-1 activity as it constitutes a promising target for attack in the search  
241 for a solution to the threat posed by late blight.

242

## 243 **Conclusion**

244 In this work we have presented the first *in silico* structural model of glucokinase-1  
245 (*PiGlcK-1*) from the phytopathogen *P. infestans*. The resulting structure was shown to be  
246 of high quality, which allows it to be used in docking analyses for other ligands. We  
247 confirmed that the folding of this protein is similar to that of other kinases from different  
248 organisms and we were able to identify the binding sites for its substrates glucose and ATP  
249 as well as for the ligands fructose, ADP and PPi reported for the first time for a classical  
250 glucokinase of the GlcK-A group. Altogether, these findings lay the groundwork for the  
251 design of future inhibitors of *PiGlcK-1* enzymatic activity that would aid in the control of  
252 late blight disease and underscored the need to establish a new classification within a more  
253 diverse group of kinases, one that considers not only the primary sequence of *PiGlcK-1*, but  
254 also its 3D structure.

255

## 256 **Acknowledgments**

257 We are very grateful to experiment.com and specially to Chralie Kinsella, Brian Repez,  
258 Amy Collete and Pureum Kim for their valuable help in financing this project.

259

## 260 **Author Contributions**

261 **Conceptualization:** Liara Villalobos-Piña, Ascanio Rojas, Héctor Acosta

262 **Formal analysis:** Liara Villalobos-Piña, Ascanio Rojas, Héctor Acosta.

263 **Funding acquisition:** Laboratorio de Fisiología, Universidad de Los Andes, Centro de  
264 Cálculo de la Universidad de Los Andes, Laboratorio de Enzimología de Parásitos,  
265 Universidad de Los Andes.

266 **Methodology:** Liara Villalobos-Piña.

267 **Project administration:** Ascanio Rojas.

268 **Supervision:** Ascanio Rojas, Héctor Acosta.

269 **Visualization:** Héctor Acosta.

270 **Writing – original draft:** Liara Villalobos-Piña

271 **Writing – review & editing:** Liara Villalobos-Piña, Ascanio Rojas, Héctor Acosta.

272

## 273 **References**

274

- 275 1. Kamoun S, Furzer O, Jones JDG, Judelson HS, Ali GS, Dalio RJD, et al. The  
276 Top 10 oomycete pathogens in molecular plant pathology. *Mol Plant Pathol.*  
277 2015;16(4):413-434
- 278 2. Haas BJ, Kamoun S, Zody MC, Jiang RHY, Handsaker RE, Cano LM, et al.  
279 Genome sequence and analysis of the Irish potato famine pathogen  
280 *Phytophthora infestans*. *Nature.* 2009;461(7262):393-398.
- 281 3. Judelson HS. Metabolic Diversity and Novelties in the Oomycetes. *Annu Rev*  
282 *Microbiol.* 2017;71(1):21-39.
- 283 4. Villalobos-Piña L, Balza H, Acosta H, Andrade-Alviarez D, Rojas A, Avilan L,  
284 et al. Characterization of Glucokinase-1 from *Phytophthora infestans*, a versatile  
285 enzyme. *Fungal Genom Biol.* 2020;10 (100001):1-9.
- 286 5. Petrey D, Honig B. Protein structure prediction: in roads to biology. *Mol Cell.*  
287 2005; 20(6):811-819.
- 288 6. Kelley L, Mezulis S, Yates C, Wass MN, Sternberg M. The Phyre2 web portal  
289 for protein modeling, prediction and analysis. *Nat Protoc.* 2015;10(6).

- 290 7. Wu S, Zhang Y. LOMETS: a local meta-threading-server for protein structure  
291 prediction. *Nucleic Acids Res.* 2007;35(10): 3375-3382.
- 292 8. Jianyi Y, Renxiang Y, Ambrish R, Dong X, Jonathan P, Yang Z. The I-  
293 TASSER Suite: protein structure and function prediction. *Nat Methods.*  
294 2015;12(1):1-5.
- 295 9. Heo L, Park H, Seok C. GalaxyRefine: protein structure refinement driven by  
296 side-chain repacking. *Nucleic Acids Res.* 2013;41
- 297 10. Maghrabi AHA, McGuffin LJ. ModFOLD6: an accurate web server for the  
298 global and local quality estimation of 3D models of proteins. *Nucleic Acids Res.*  
299 2017; 45:W416-W421.
- 300 11. Waterhouse A, Bertoni M, Bienert S, Studer G, Tauriello G, Gumienny R, Heer  
301 FT, de Beer TAP, Rempfer C, Bordoli L, Lepore R, Schwede T. SWISS-  
302 MODEL: homology modelling of protein structures and complexes. *Nucleic*  
303 *Acids Res.* 2018; 46:W296-W303.
- 304 12. Stivala A, Wybrow M, Wirth A, Whisstock JC, Stuckey PJ. Automatic  
305 generation of protein structure cartoons with Pro-origami. *Bioinformatics.* 2011;  
306 27(23):3315-3316.
- 307 13. Pettersen EF, Goddard TD, Huang CC, Couch GS, Greenblatt DM, Meng EC, et  
308 al. UCSF Chimera a visualization system for exploratory research and analysis.  
309 *J Comput Chem.* 2004; 25:1605-1612.
- 310 14. Grosdidier A, Zoete V, Michielin O. SwissDock, a protein-small molecule  
311 docking web service based on EADock DSS. *Nucleic Acids Res.* 2011; 39:  
312 W270-W277.
- 313 15. Kim S, Chem J, Cheng T, Gindulyte A, He S, Li Q. PubChem, in 2021: new  
314 data content and improved web interfaces. *Nucleic Acids Res.* 2021; 49(D1):  
315 D1388-D1395.
- 316 16. Zhang J, Li C, Shi T, Chen K, Shen X, Jiang H. Lys169 of human Glucokinase is  
317 a determinant for glucose phosphorylation: implication for the atomic  
318 mechanism of glucokinase catalysis. *PLoS One.* 2009;4(7):1-12.

- 319 17. Nagata R, Fujihashi M, Sato P, Atomi H, Miki K. Identification of a  
320 pyrophosphate-dependent kinase and its donor selectivity determinants. Nat  
321 Commun. 2018;9: 1765:1-8.
- 322 18. Park J, Gupta RS. Adenosine kinase and ribokinase-the RK family of proteins.  
323 Cell Mol Life Sci. 2008;65:2875-2896.
- 324 19. Cabrera R, Babul J, Guixé V. Ribokinase family evolution and the role of  
325 conserved residues at the active site of the PfkB subfamily representative, Pfk2  
326 from *Escherichia coli*. Arch Biochem Biophys. 2010;502:23-30.
- 327 20. Van Schaftingen E. Hexokinase/Glucokinase. Encyclopedia of Biochemistry 3<sup>rd</sup>  
328 Edition. 2020. doi:10.1016/B978-0-12-819460-7.00034-7.
- 329 21. Lunin VV, Li Y, Schrag JD, Iannuzzi P, Cygler M, Matte A. Crystal structures  
330 of *Escherichia coli* ATP-dependent glucokinase and its complex with glucose. J  
331 Bacteriol. 2004;186(20):6915-6927.
- 332 22. Ito S, Fushinobu S, Jeong J, Yoshioka I, Koga S, Shoun H, et al. Crystal  
333 structures of an ADP-dependent glucokinase from *Pyrococcus furiosus*.  
334 Implications for a sugar-induced conformational change in ADP-dependent  
335 kinase. J Mol Biol. 2003;(331):871-883.
- 336 23. Engstrom K, Stromberg A. Changes in sugar content during induction of  
337 systemic acquired resistance to late blight caused by *Phytophthora infestans*  
338 (Mont) de Bary in potato. J Phytopathol. 1996;144: 33–36.
- 339 24. Daniele E, Dommès J, Hausman, JF. Carbohydrates and resistance to  
340 *Phytophthora infestans* in potato plants. Acta Physiol Plant. 2003;25: 171–178.
- 341 25. Judelson HS, Tani S, Narayan RD. Metabolic adaptation of *Phytophthora*  
342 *infestans* during growth on leaves, tubers and artificial media. Mol Plant Pathol.  
343 2009;10(6):843-855.
- 344 26. García-Bayona L, Garavito MF, Lozano GL, Vasquez JJ, Myers K, Fry WE,  
345 Bernal A, Zimmermann BH, Restrepo S. *De novo* pyrimidine biosynthesis in the  
346 oomycete plant pathogen *Phytophthora infestans*. Gene. 2014;537(2):312-321.
- 347 27. Ah-Fong AM, Kim KS, Judelson HS. RNA-seq of life stages of the oomycete  
348 *Phytophthora infestans* reveals dynamic changes in metabolic, signal

- 349 transduction, and pathogenesis genes and a major role for calcium signaling in  
350 development. BMC Genomics. 2017;18(198):1-21.
- 351 28. Marshall J, Anthony R, Ashton A. Isolation and characterization of four genes  
352 encoding pyruvate, phosphate dikinase in the oomycete plant pathogen  
353 *Phytophthora cinnamomi*. Curr Genet. 2001; (1):73–81.
- 354 29. Abrahamian M, Kagda M, Ah-Fong AM, Judelson HS. Rethinking the evolution  
355 of eukaryotic metabolism: novel cellular partitioning of enzymes in  
356 stramenopiles links serine biosynthesis to glycolysis in mitochondria. BMC  
357 Evol Biol. 2017; 17(241):1-16.
- 358 30. Okorokov LA, Sysuev VA, Kulaev IS. Pyrophosphate-stimulated uptake of  
359 calcium into the germlings of *Phytophthora infestans*. Eur J Biochem. 1978;  
360 83:507- 511.

361  
362  
363  
364  
365  
366  
367

368 **Table 1.** Models built by various servers and their evaluation results.

<i>Model</i>	<i>Favored region (%)</i>	<i>Confidence and p-value</i>	<i>Global model quality score</i>
Phyre2			
Before refinement	91.50	4.42 E-7	0.6220
After refinement <sup>a</sup>	97.95	1.93 E-7	0.6412
LOMETS			
Before refinement	93.45	5.14 E-8	0.6718
After refinement <sup>b</sup>	96.30	5.22 E-8	0.614
I-TASSER			
Before refinement	81.60	3.56 E-8	0.6803
After refinement <sup>c</sup>	96.01	2.83 E-8	0.6854

369 <sup>a</sup> 2 time, <sup>b</sup> 3 time, <sup>c</sup> 3 time  
370

371 **Figure Legends**

372

373 **Fig. 1. Ramachandran plot of *PiGlcK-1* model for Phyre2 before (A) and after (B)**  
374 **refinement.**

375

376 **Fig. 2. *PiGlcK-1* model 3D predicted by Phyre2.** *PiGlcK-1* monomer showing the  
377 glucose binding motif in the major lobe, the ATP binding motif in the minor lobe and the  
378 catalytic aspartate binding motif in the hinge region.

379

380 **Fig. 3. The binding site region between *PiGlcK-1* and glucose and ATP.** Docking result  
381 using Swiss Dock. Amino acids in *PiGlcK-1* involved in the interaction with their ligands  
382 are highlighted in red (ATP) and blue (glucose). Catalytic aspartate is highlighted in green.

383

384 **Fig. 4. Docking result using Swiss Dock for fructose (A) and ADP (B) to *PiGlcK-1*.** (A)  
385 Amino acids in *PiGlcK-1* involved in the interaction with their ligands are highlighted in  
386 red (ATP) and blue (fructose). (B) Amino acids in *PiGlcK-1* involved in the interaction  
387 with their ligands are highlighted in red (ADP) and blue (glucose).

388

389 **Fig. 5. Docking result using Swiss Dock for PPI to *PiGlcK-1*.** (A) Overview of the PPI  
390 binding site (orange) distinct from that of ATP (red) and glucose (blue). (B) Close-up of the  
391 PPI binding region showing the GXGE motif and specific amino acids involved in PPI  
392 recognition.

393

394 **Supplementary data**

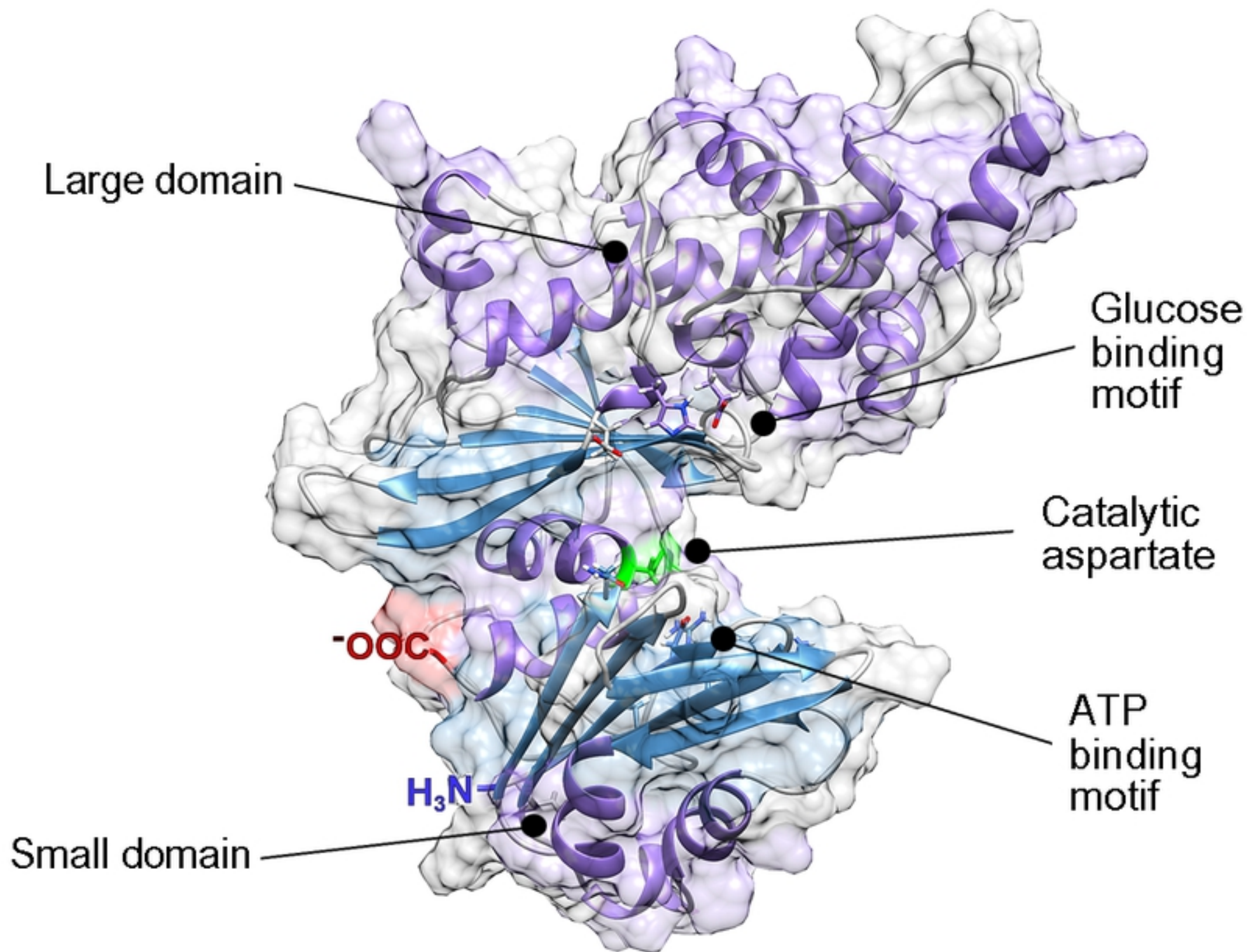
395



396 **S1. Fold topology of *PiGlcK-1* monomer obtained by Pro-Origami.** Topology of *P.*  
397 *infestans* with two domains (light blue shading), composed of lamellae  $\beta$ -sheet (dark blue)  
398 and flanked by  $\alpha$ -helices (purple).

399

400



Figure

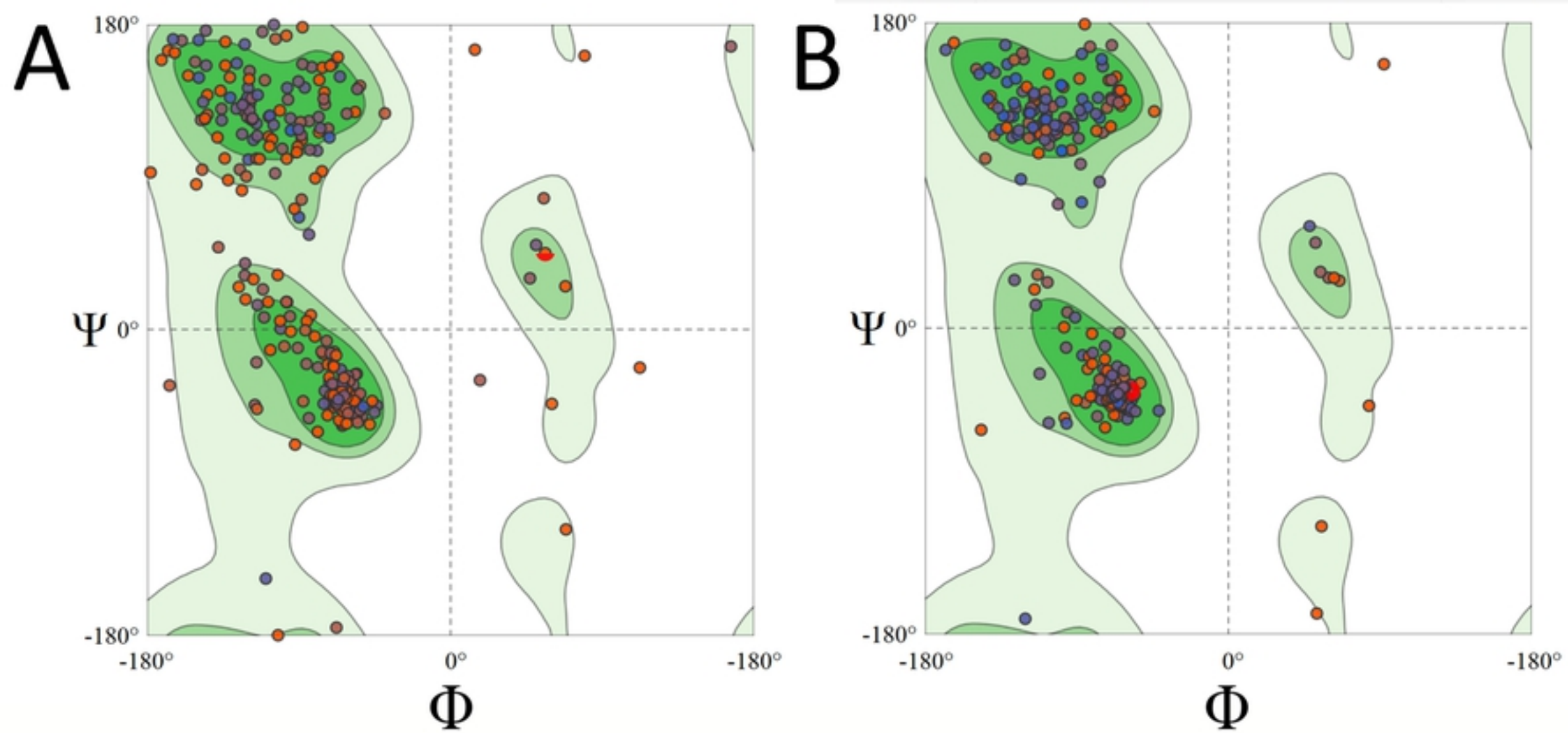


Figure 1

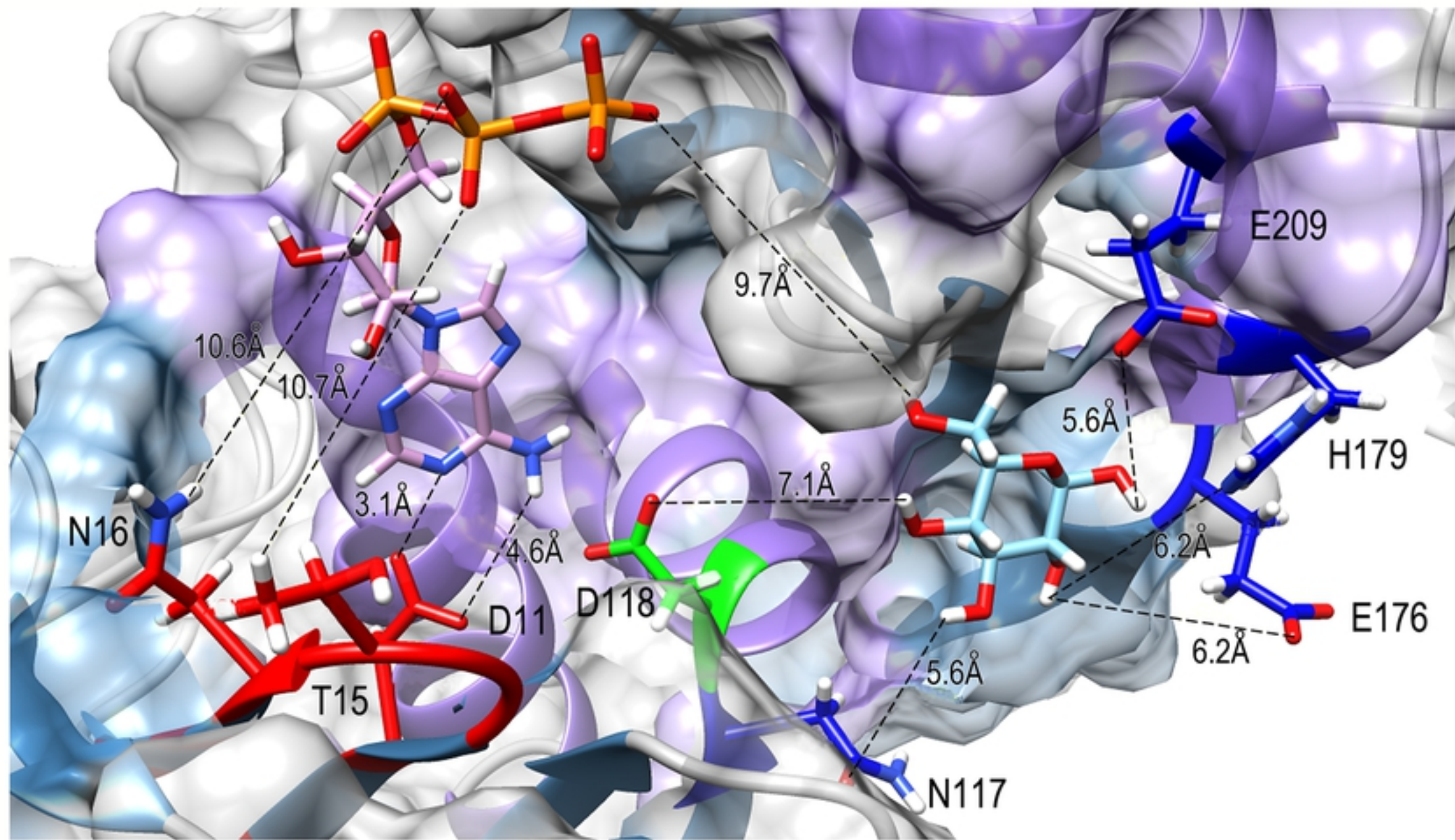


Figure 3

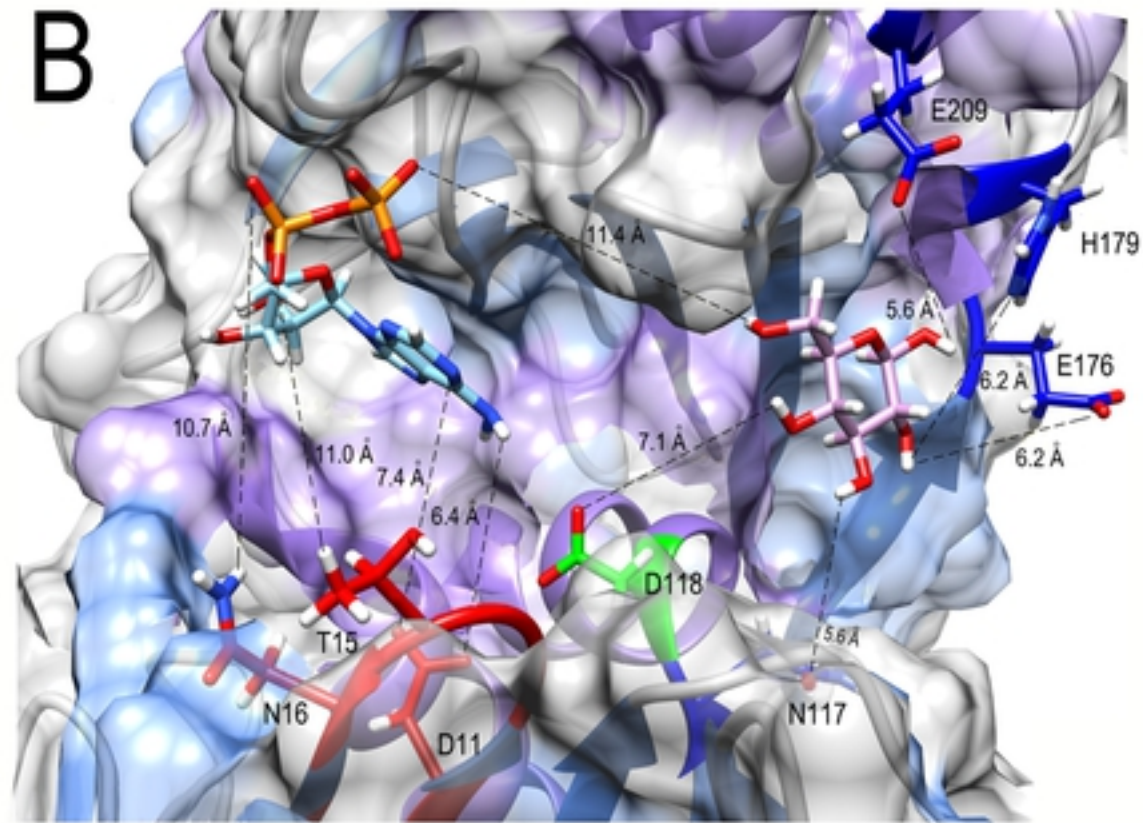
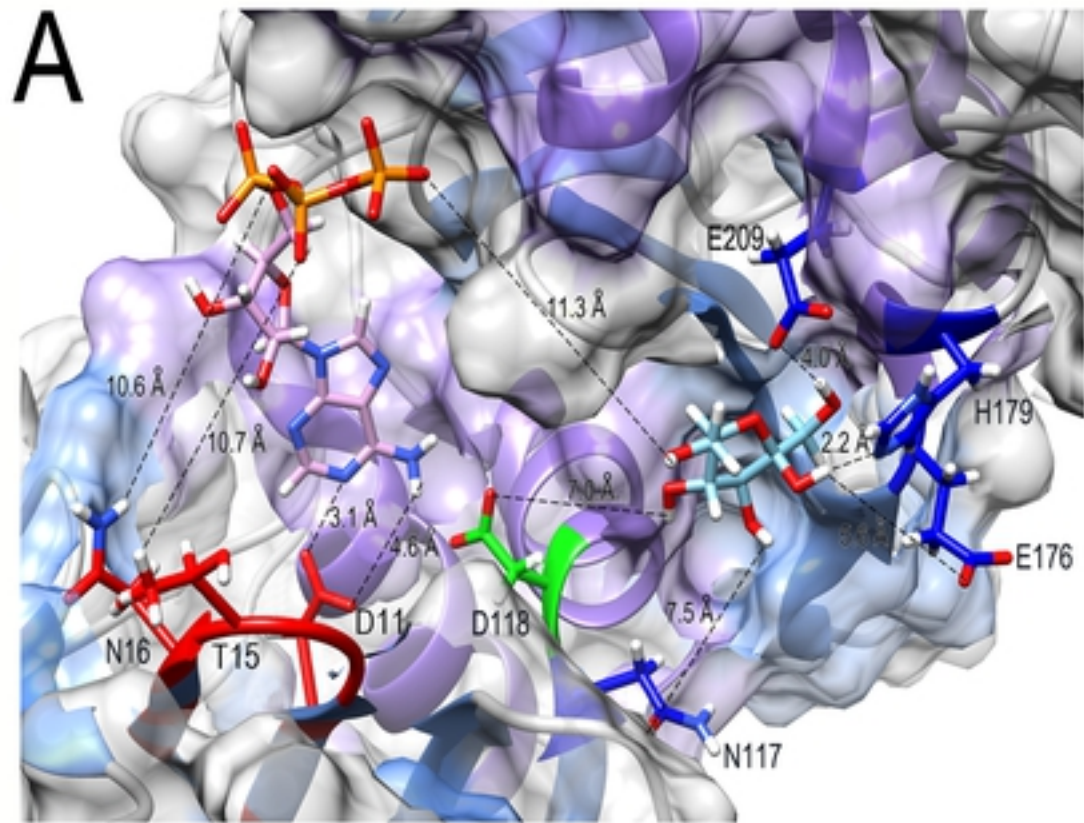


Figure 4

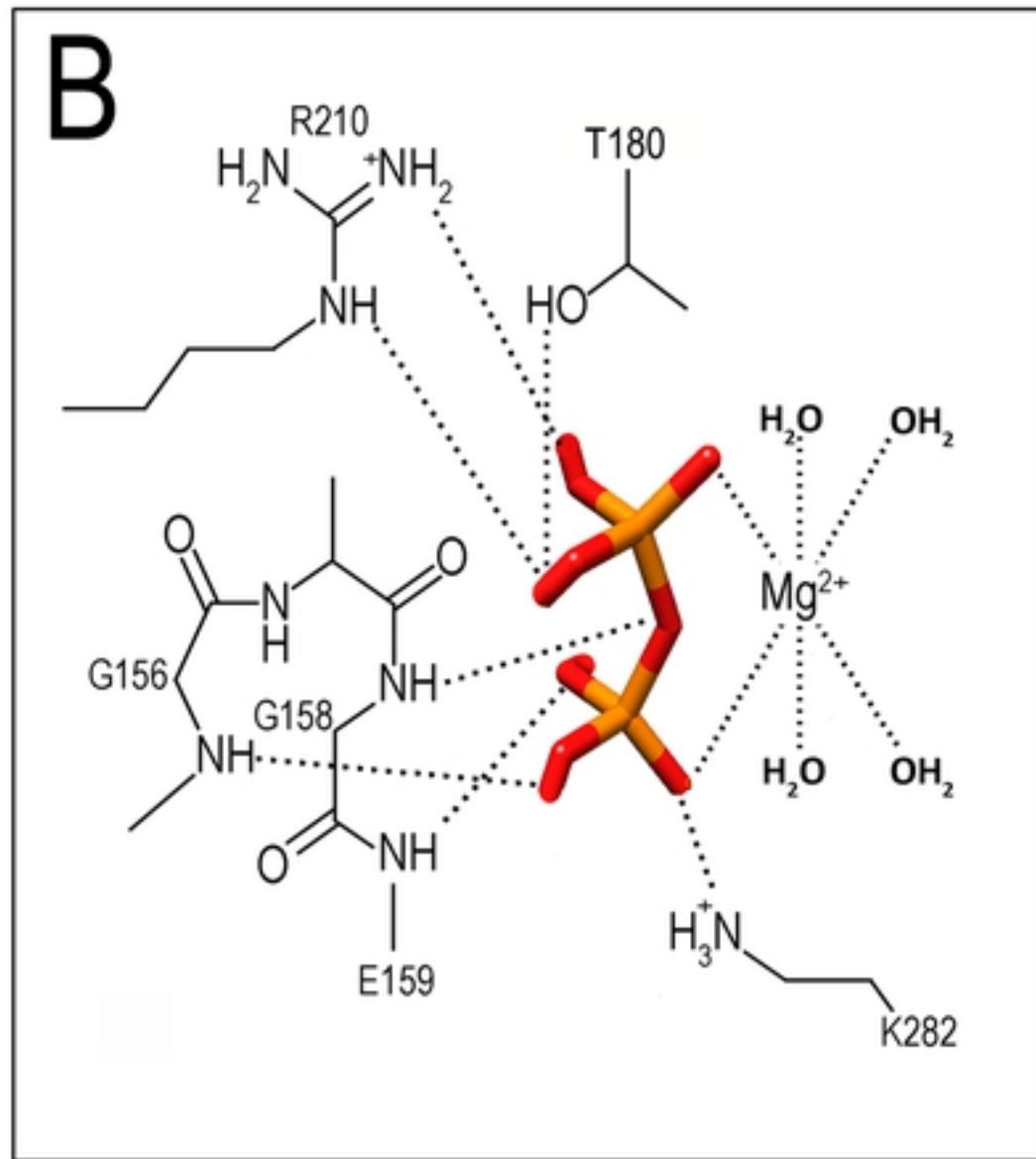
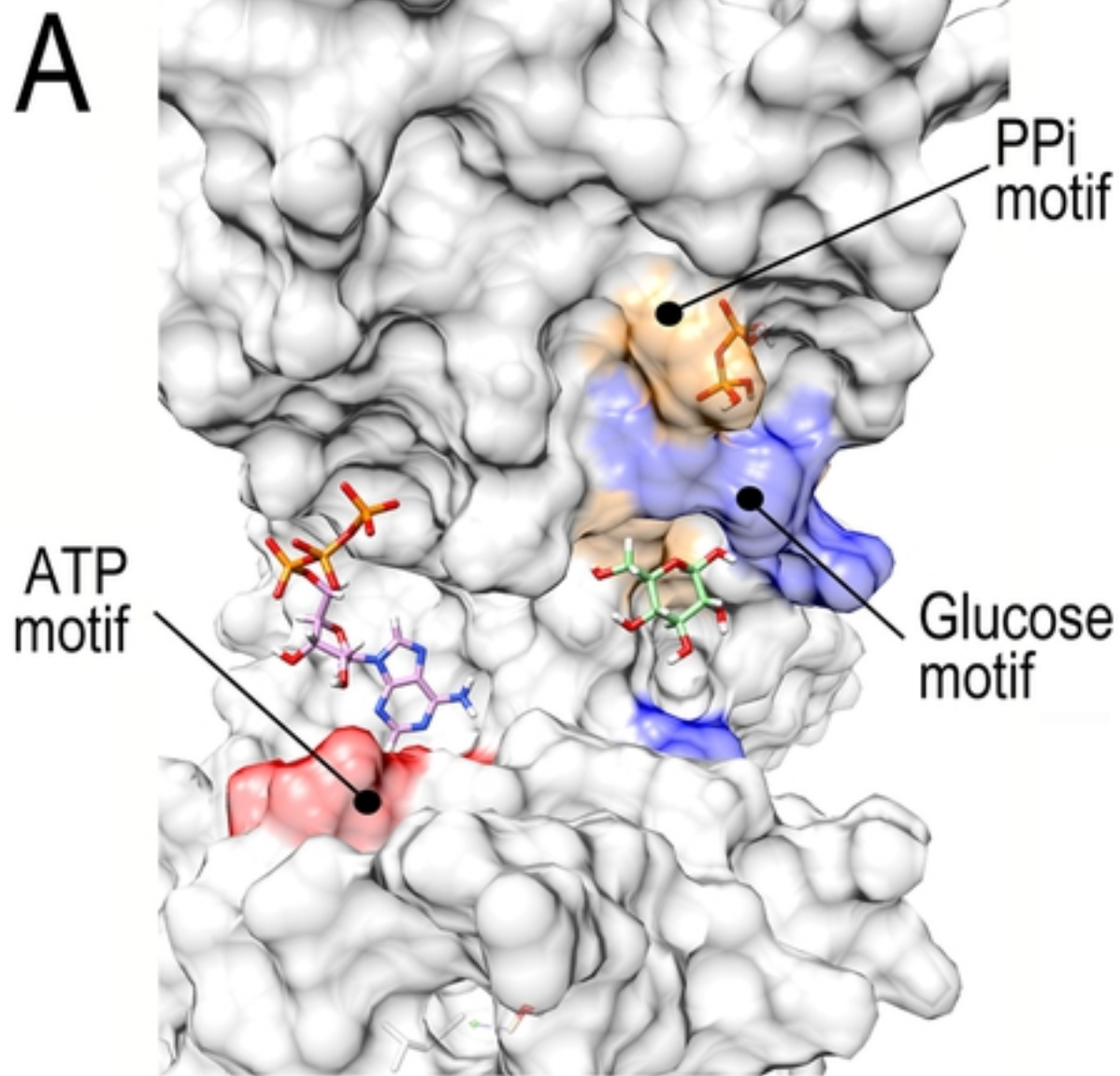


Figure 5

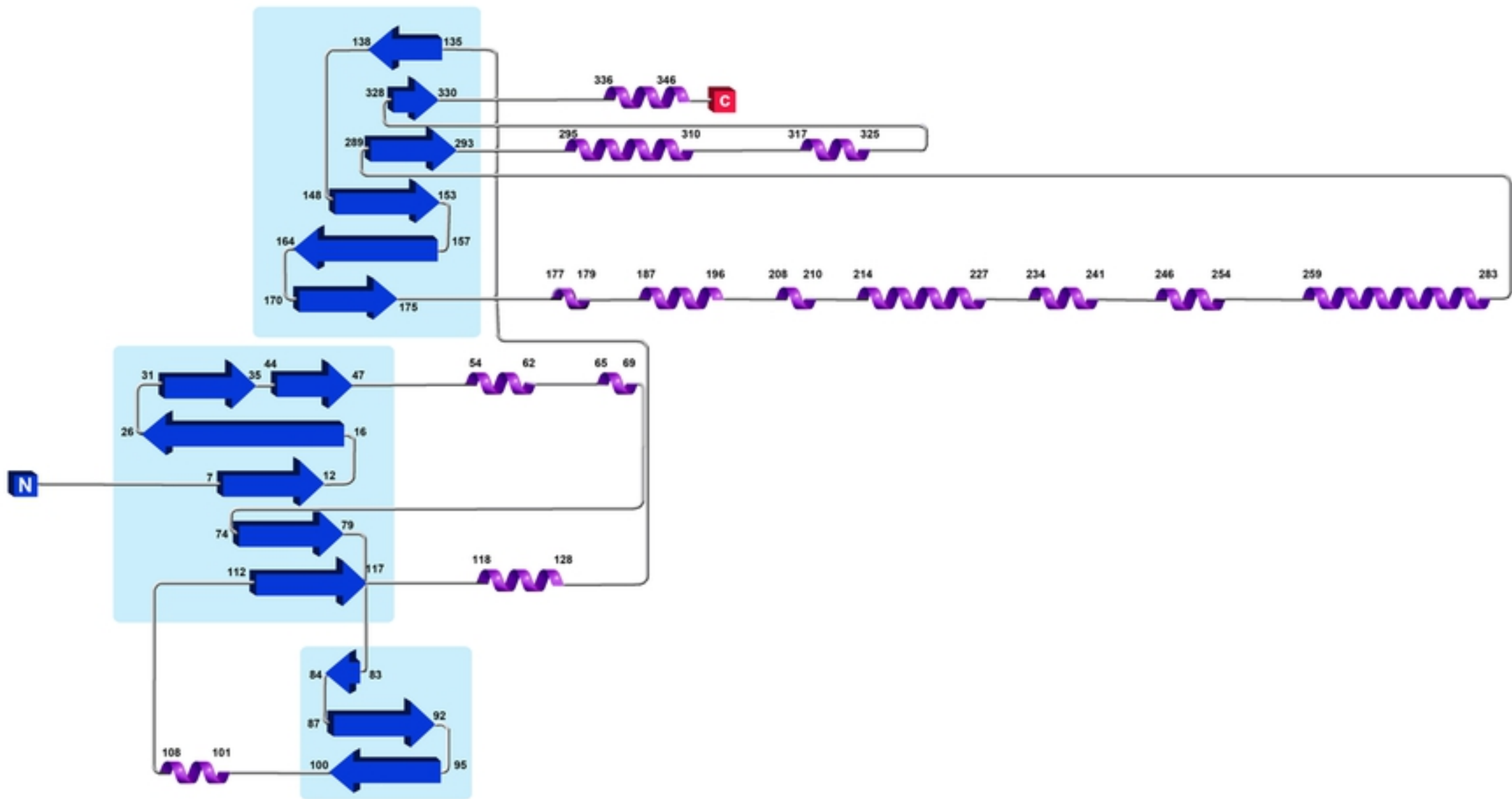


Figure S1